Revisiting a hydrological analysis framework with International Satellite Land Surface Climatology Project Initiative 2 rainfall, net radiation, and runoff fields

Randal D. Koster,[1] Balázs M. Fekete,[2] George J. Huffman,[3] and Paul W. Stackhouse Jr[4]

Received 9 February 2006; revised 17 July 2006; accepted 4 August 2006; published 23 November 2006.

[1] The International Satellite Land Surface Climatology Project Initiative 2 (ISLSCP-2) data set provides the data needed to characterize the surface water budget across much of the globe in terms of energy availability (net radiation) and water availability (precipitation) controls. The data, on average, are shown to be consistent with Budyko's decades-old framework, thereby demonstrating the continuing relevance of Budyko's semiempirical relationships. This consistency, however, appears only when a small subset of the data with hydrologically suspicious behavior is removed from the analysis. In general, the precipitation, net radiation, and runoff data also appear consistent in their interannual variability and in the phasing of their seasonal cycles.

Citation: Koster, R. D., B. M. Fekete, G. J. Huffman, and P. W. Stackhouse Jr. (2006), Revisiting a hydrological analysis framework with International Satellite Land Surface Climatology Project Initiative 2 rainfall, net radiation, and runoff fields, *J. Geophys. Res.*, *111*, D22S05, doi:10.1029/2006JD007182.

1. Introduction

[2] The International Satellite Land Surface Climatology Project Initiative 2 (ISLSCP-2) data set [*Hall et al.*, 2006] provides global, coregistered, high-resolution ($1^\circ \times 1^\circ$) fields of land surface meteorological and hydrological data for scientific analysis. Naturally, many of the variables in the data set are intrinsically related to each other. This raises the question of data consistency: given that different measurement systems are used to generate, for example, the rainfall and runoff components of the data set, are the values provided for these two variables mutually consistent? To address this question, the variables must be examined jointly in a sensible way.

[3] *Budyko* [1958, 1974] pioneered the joint analysis of land surface hydroclimatological variables. He recognized that evaporation from the land surface requires both water at the surface and incident energy at the surface, the latter for the change in phase of water. Mean annual evaporation (E), he argued, is thus effectively controlled by two things: the mean annual precipitation (P) and the mean annual net radiation (R_{net}). When $P \ll R_{net}/\lambda$, where λ is the latent heat of vaporization, the evaporation is water limited, and $E \approx P$. On the other hand, when $P \gg R_{net}/\lambda$, the evaporation is energy limited, and $E \approx R_{net}/\lambda$. When P and R_{net}/λ are of the same order, E will be lower than both, since additional issues then come into play. In essence, Budyko realized that a region's water balance cannot be estimated from precipitation or net radiation data alone; the two forcings must be considered together in a single framework.

[4] The joint controls are summarized in Budyko's plot of E/P versus dryness index D, defined as $D = R_{net}/P\lambda$ (Figure 1). The solid curve in Figure 1 is defined by the equation

$$\mathrm{E/P} = \mathcal{F}(\mathrm{D}) = [\mathrm{D}\ (\tanh\ 1/\mathrm{D})(1 - \cosh\ \mathrm{D} + \sinh\ \mathrm{D})]^{1/2} \quad (1)$$

The curve is a semiempirical fit to the limited observations available to Budyko when he performed his analysis. When D is large, water-limited conditions prevail, and the curve approaches the horizontal line (equivalent to the condition $E = P$). When D is small, energy-limited conditions prevail, and the curve approaches the 1:1 line, equivalent to the condition $E = R_{net}/\lambda$. For all values of D, the curve allows a first-order estimate of the annual evaporation rate.

[5] The curve works well on average for the regions investigated by *Budyko* [1974], and it describes well the evaporation rates generated by various atmospheric general circulation models [*Koster et al.*, 2001]. As a research framework, it can be used to understand interannual variations in the water cycle; *Koster and Suarez* [1999] use (1) to derive the following equation for the standard deviation of annual evaporation, σ_E:

$$\sigma_\mathrm{E}/\sigma_\mathrm{P} = \mathcal{F}(\mathrm{D}) - \mathrm{D}F'(\mathrm{D}) \quad (2)$$

where σ_P is the standard deviation of annual precipitation, $\mathcal{F}(\mathrm{D})$ is the function described in (1), and $F'(\mathrm{D})$ is the first derivative of $\mathcal{F}(\mathrm{D})$ with respect to D. Equation (2),

[1]Global Modeling and Assimilation Office, NASA Goddard Space Flight Center, Greenbelt, Maryland, USA.
[2]Water Systems Analysis Group, Complex Systems Research Center, Institute for the Study of Earth, Oceans, and Space, University of New Hampshire, Durham, New Hampshire, USA.
[3]Science Systems and Applications, Inc., NASA Goddard Space Flight Center, Greenbelt, Maryland, USA.
[4]NASA Langley Research Center, Hampton, Virginia, USA.

0148-0227/06/2006JD007182

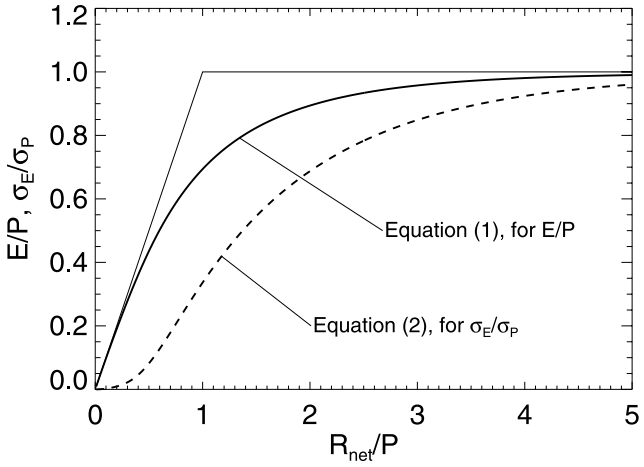

Figure 1. Curves derived by *Budyko* [1958] for E/P and *Koster and Suarez* [1999] for σ_E/σ_P.

illustrated by the dotted line in Figure 1, successfully characterizes the interannual variability of evaporation in a number of AGCMs [*Koster et al.*, 2001].

[6] Although Budyko's semiempirical relationships are useful for characterizing first-order controls on the mean and variability of annual evaporation and runoff and for guiding further inquiry into the global surface water balance, they have rarely been tested on a global scale using purely observational data. *Milly and Dunne* [2002], as part of a broad analysis addressing controls on runoff variability, examined observed precipitation, radiation, and runoff data over a number of basins across the globe and found some discrepancies between the observations and Budyko-based estimates of evaporation. Now, with the advent of the global $1^\circ \times 1^\circ$ ISLSCP-2 observational data set, we can test the Budyko framework even more comprehensively. Several questions suggest themselves: Do Budyko's relationships still hold up? Is the framework still valid for exploring controls on global hydrology? Can the framework be used to identify deficiencies or inconsistencies in the data sets? In this paper, we use the ISLSCP-2 precipitation, net radiation, and runoff fields to revisit and reevaluate Budyko's framework. We describe the data sets used in section 2, and we identify some clear inconsistencies and some suspicious behavior among the data in section 3. In section 4, we test the Budyko framework with the global data.

2. Data Used

2.1. Precipitation

[7] The Global Precipitation Climatology Project (GPCP) Version 2 Satellite-Gauge (SG) precipitation data set, consisting of globally complete $2.5^\circ \times 2.5^\circ$ monthly estimates, is based on a variety of satellite data sets plus gauge analyses [*Adler et al.*, 2003] (see also ftp://precip.gsfc.nasa.gov/pub/gpcp-v2/doc/V2_doc). The SG data set extends from 1979 to present. Beginning in July 1987, but not including December 1987, the data set incorporates Special Sensor Microwave/Imager (SSM/I) passive microwave estimates at low latitudes and midlatitudes and Television-Infrared Observation Satellite (TIROS) Operational Vertical Sounder (TOVS) estimates at higher latitudes. Over the latitude band 40°N-S, infrared brightness temperatures (IR T_bs) are converted into precipitation estimates by applying the Adjusted Geostationary Operational Environmental Satellite (GOES) Precipitation Index (AGPI [*Adler et al.*, 1994]), which depends on calendar month calibrations computed with approximately time/space matched IR T_b's and SSM/I rain estimates. A MultiSatellite (MS) estimate is composited from these inputs, and then the SG product is produced in two steps: (1) The MS estimate is adjusted to the large-scale gauge average for each grid box over land. (2) The gauge-adjusted MS estimate and the gauge analysis are combined in a weighted average, where the weights are the inverse (estimated) error variance of the respective estimates.

[8] The period before the start of SSM/I observations requires a more approximate scheme. During the period 1986 to June 1987, plus December 1987, outgoing longwave radiation (OLR) precipitation index (OPI) data are climatologically calibrated by the 1988–1996 GPCP SG estimates and used in place of the SSM/I–TOVS component. The MS field is built from geo-AGPI estimates where available (40°N-S) and calibrated OPI estimates elsewhere, and the results are combined with the gauge data as in the recent era to produce the SG product.

[9] *Hall et al.* [2006] provide a discussion of SG data quality specifically directed at ISLSCP-2 users. The ancillary data documentation and supplemental fields (e.g., rain gauge density) provided by ISLSCP-2 contain important additional information on the precipitation data's uncertainty. This uncertainty has many sources: a lack of gauges in many parts of the world; the tendency to locate gauges in developed areas (e.g., in the valleys rather than at high elevations, where more of the rain falls); inhomogeneity in instrumentation and reporting methods; and uneven skill by remote sensing algorithms, which have particular difficulties, for example, over frozen surfaces. Overall, the data we examine here tend to be more uncertain in mountains, deserts, high latitudes, and areas lacking development and/or suffering societal upheavals. Biases, however, are considered relatively small, even in gauge-sparse regions. The exception is in mountainous regions, where the gauge (and therefore the SG product) will generally underestimate the true precipitation because of the aforementioned biased siting of gauges. The data account explicitly for gauge undercatch.

2.2. Net Radiation

[10] The Surface Radiation Budget (SRB) project at NASA is a component of the Global Energy and Water Cycle Experiment (GEWEX), under the auspices of the World Climate Research Programme (WCRP). SRB produces estimates of surface radiative flux quantities by processing satellite observations, reanalysis meteorology, and ozone measurements through parameterized radiation models. For the ISLSCP-2 data set, monthly averaged SRB (Release 2.0) solar (SW, or shortwave) and thermal infrared (LW, or longwave) data [*Cox et al.*, 2004; *Stackhouse et al.*, 2004] were supplied at a resolution of 1° latitude $\times$ 1° longitude with the algorithms described below.

[11] The radiation fluxes for ISLSCP-2 were computed using the International Satellite Cloud Climatology Project (ISCCP) "DX" data [*Rossow and Schiffer*, 1999], using an

averaging approach analogous to that of *Rossow et al.* [1996] to produce cloud and surface properties at a 1° spatial and 3-hourly temporal resolution. The needed meteorological profile information (e.g., temperature and humidity) was provided by the Goddard Earth Observing System (GEOS) v.1 reanalysis [*Schubert et al.*, 1995], which was generated by the Data Assimilation Office (DAO, now the Global Modeling and Assimilation Office) of NASA's Goddard Space Flight Center. Additional data used include the 1.25° longitude × 1° latitude column ozone fields derived from Total Ozone Mapping Spectrometer (TOMS) data. High-resolution classification maps of land surface type helped in the assignment of surface spectral albedo and emissivities [*Charlock and Alberta*, 1996; *Wilber et al.*, 1999].

[12] The shortwave fluxes submitted to ISLSCP-2 were computed from an upgraded version of the algorithm of *Pinker and Ewing* [1985]. This algorithm computes a broadband solar flux for each time stamp using a spectral two-stream delta-Eddington model to map broadband reflected fluxes at the top of the atmosphere (TOA) to transmitted fluxes at the surface. The reflected fluxes at TOA are computed using narrowband-to-broadband relationships on the visible radiances and angular distribution models (ADMs) from the Earth Radiation Budget Experiment (ERBE). The broadband surface albedo is retrieved at every step using the ISCCP background surface radiance and assumed column aerosol, precipitable water and column ozone. The spectral shape of the albedo is fixed according to the surface type prevalent in the grid box. This surface albedo is then used to infer the transmitted flux, weighing the contributions of cloudy and clear-sky fluxes. The surface albedo and the transmitted flux are used to infer the reflected surface flux of the grid box. The model has been updated with new water vapor parameterizations and averaging schemes.

[13] The SRB SW Release 2.0 monthly averaged fluxes were compared to surface measurements across the globe from the Baseline Surface Radiation Network (BSRN [*Ohmura et al.*, 1998]) and the Global Energy Balance Archive (GEBA [*Gilgen and Ohmura*, 1999]). Comparisons to the GEBA data set suggest that the SRB downwelling fluxes have a bias and RMSE of 1.8% and 15.2%, respectively, whereas comparisons with the BSRN data suggest a bias and RMSE of −2.2% and 14.3%, respectively. Estimating errors in upward fluxes from surface measurements is problematic because of spatial heterogeneity, so we estimate the uncertainty in the net fluxes using the above comparisons between the downwelling fluxes and flux albedo differences between SRB and ISCCP-FD [*Zhang et al.*, 2004], as documented by *Zhang et al.* [2006]. *Zhang et al.* [2006] show that SRB albedos in snow-free regions are 2% higher (4.6% standard deviation) than ISCCP-FD values. For snow covered landmass areas, the differences are much larger, and SRB albedos are 11.2% (8.3% standard deviation) lower than ISCCP-FD values. However, subsequent analysis shows that ISCCP-FD and SRB differences in the downwelling SW tend to compensate for albedo differences. Using these differences as a proxy for the uncertainty in the SRB surface SW net fluxes, the uncertainty range is expected to be within ±10 W m^{-2} overall (about 8% of the globally averaged surface net flux), with the largest uncertainties over snow covered areas. However, because the polar regions are excluded from this study, much of these snow covered areas are not considered. Last, we note that SW errors vary with altitude to a maximum negative bias of 50 W m^{-2} in summer in the Tibetan plateau region. In this case, the surface albedo was also too low so that the net flux is more likely to be biased high.

[14] For the ISLSCP-2 longwave fluxes, the GEWEX SRB Longwave Quality Check algorithm was used (SRB Rel. 2.0). This algorithm, a slightly upgraded version of the algorithm of *Gupta et al.* [1999], uses broadband parameterizations of narrow band (10 cm^{-1}) radiative transfer calculations to compute a clear-sky longwave flux given the meteorological profile (water vapor and temperature) of the grid box. The model uses cloud fraction and the cloud top temperatures to prescribe the effects of clouds on the clear-sky downwelling flux. TOA fluxes are currently not computed with this algorithm, but the model does allow for nonblack surface emittances. These nonblack broadband surface emittances are used in conjunction with the diurnally varying GEOS-1 surface temperatures to compute the upwelling longwave fluxes.

[15] When the ISLSCP downwelling longwave fluxes are compared to BSRN measurements (from 1992 to 1995), the mean bias is about 5 W m^{-2} (with model fluxes higher), and the random error is about ±15 W m^{-2}. This mean bias is considered to be within the uncertainty for BSRN measurements. On the basis of estimates of surface temperature reliability for the GEOS-1 modeling system, we infer a mean bias of order ±2–4 W m^{-2} and an RMSE of about 12–18 W m^{-2} for the upwelling longwave fluxes in the ISLSCP data set. The LW net fluxes are estimated to be within 10 W m^{-2} of truth, with the largest potential errors in drier areas over snow covered surfaces.

[16] For the present paper, we utilize an SRB product that represents a combination of the solar and longwave fluxes at the surface: the net radiation at the surface, R_{net}. This flux is simply the sum of the net shortwave and net longwave fluxes. Throughout the text, we normalize the R_{net} values with the latent heat of vaporization, λ, taken here to be 2.45×10^6 J/kg (a value typical of liquid-vapor phase changes at the surface of the Earth). As discussed in section 1, the normalization allows the net radiation to be expressed in terms of the amount of water it can evaporate. The latent heat of vaporization is about 15% larger for evaporation from snow (sublimation). For simplicity (and because the ISLSCP-2 precipitation data are not partitioned into rainfall and snowfall data), this difference is ignored in the present study. A simple test in which winter midlatitude R_{net} values were normalized by the higher latent heat of sublimation showed very little impact of this change on this study's results.

2.3. Runoff

[17] The gridded runoff data set included in the ISLSCP-2 archive is an update to the UNH-GRDC composite runoff fields of *Fekete et al.* [2002], a data set that combines observed river discharge from the Global River Data Center (GRDC) with simulated water balance model (WBM) estimates. (A runoff value for a given cell represents the runoff generated within the cell only and does not include runoff flowing into the cell from upstream.) In essence,

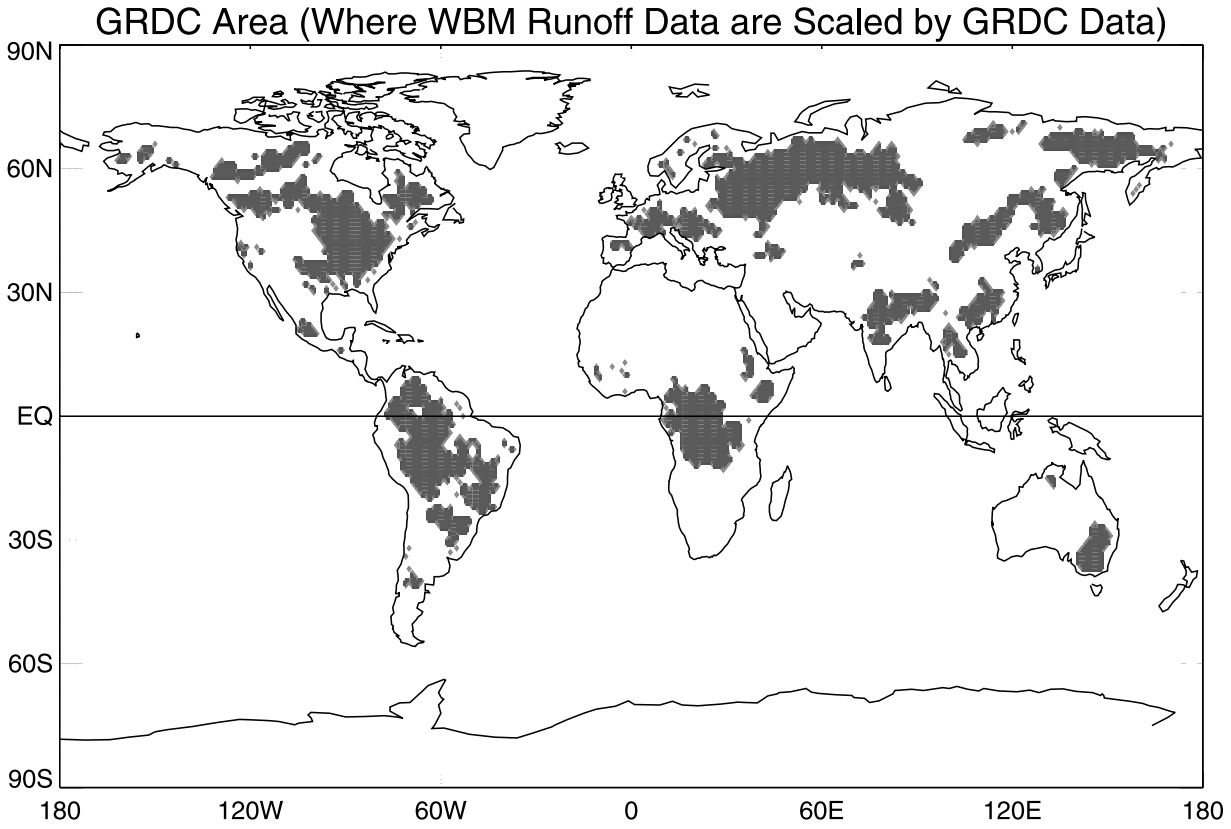

Figure 2. Locations (shaded) where the raw WBM runoff data have been "corrected" for the ISLSCP-2 data set through a scaling with observed stream gauge measurements, as archived by GRDC.

WBM estimates were "corrected" with the GRDC data through the application of scaling factors, factors that forced the gridded WBM annual estimates across gauged areas to sum up to the corresponding observed discharge values. The corrections were computed from annual totals and thus did not affect the seasonality of the WBM estimates.

[18] The original UNH-GRDC data set (http://www.grdc.sr.unh.edu) consists of monthly climatologies at $0.5^\circ \times 0.5^\circ$ spatial resolution. To generate the fields for ISLSCP-2, the raw WBM monthly means were revised through the application of climate forcing (air temperature, precipitation, vapor pressure, solar radiation, wind speed) from the Climate Research Units (CRU) data set [*New et al.*, 1999, 2000]. In addition, a 10-year monthly time series of runoff for the 1986–1995 period was developed for ISLSCP-2.

[19] Of course, GRDC streamflow observations do not span the Earth's land area. In nonmonitored regions, the runoff estimates are derived from WBM estimates alone. Furthermore, in monitored regions, GRDC corrections were not applied when GRDC and WBM data values appeared inconsistent. Potential reasons for inconsistencies between GRDC measurements and the raw WBM estimates are many. For example, although discharge is thought to be the most accurately measured component of the hydrological cycle, the uncertainty of discharge increments (the difference in discharge between adjacent stream gauges) can be large. (For reference, the discharge measurements at the gauges have an accuracy of 5–20% [*Hageman and Dümenil*, 1998; *Rantz et al.*, 1982].) Also, WBM runoff estimates are subject to uncertainty in measured precipitation fields, and observed discharge may be influenced by human activities such as water withdrawal, interbasin transfer, and reservoir operation (though reservoir operation probably has a small impact on the long-term mean annual discharge). For both the climatology and the 10-year time series, the WBM estimates were scaled with GRDC data only if the scaling factor was in the 0.5–2.0 range. Regions with scaling factors outside this range were left uncorrected, reflecting (in part) our lack of knowledge regarding which data set is better.

[20] We restrict our analyses below to regions for which the GRDC scaling factors are applied, that is, to regions for which the WBM runoff estimates are indeed corrected with stream gauge measurements. These regions are illustrated in Figure 2. The corrected long-term averages in the shaded areas of Figure 2 were determined from at least five GRDC-corrected years of $1^\circ \times 1^\circ$ data. (A $1^\circ \times 1^\circ$ data value was considered "corrected" if all four contributing $0.5^\circ \times 0.5^\circ$ quadrants were themselves corrected.) If a grid cell included years of data that were not scaled with GRDC measurements, those years were not used to compute the averages.

3. Regions and Time Period Considered

3.1. GRDC-Corrected Basins

[21] The aim of the present paper is to examine independently measured precipitation, net radiation, and runoff values to evaluate their mutual consistency within the Budyko framework. Note that the runoff and precipitation

data in the unshaded land areas of Figure 2 are not truly independent of each other, since the runoff values are derived solely from the WBM analysis, an analysis that uses observed precipitation as an input. Only the runoff in the shaded areas of Figure 2 can be considered largely independent of the precipitation measurements, since the long-term runoff means there are scaled to GRDC stream gauge measurements (see section 2.3). Thus, for the present study, we utilize only data from the shaded areas in Figure 2.

[22] The hydrological regimes of the stream gauge monitored and nonmonitored areas (the shaded and unshaded land areas in Figure 2) are substantially different. For the original UNH-GRDC composite runoff data set, *Fekete et al.* [2002] show that roughly 60% of the nonmonitored landmass is dry (without any organized river network), implying that the remaining 40% of the nonmonitored land area must be substantially wetter than the monitored land area, since the monitored and nonmonitored areas for that data set are roughly equal in area and produce about the same discharge to the oceans. While the monitored area is smaller for the ISLSCP version of the data (due, for example, to differences in data period), the nonmonitored area in Figure 2 still shows a distinct relative prevalence of deserts.

3.2. Points With Hydrologically Inconsistent Data

[23] Data within a handful of ISLSCP-2 land grid cells, roughly 2% of all land grid cells (and roughly 3% of the grid cells within the GRDC-corrected area) show a clear hydrological inconsistency: The long-term average of the locally generated runoff, Q, in these cells exceeds the long-term average precipitation, P. These cells are marked with a dot in Figure 3a. The runoff Q does not exceed P by more than 10% in about a third of the marked cells, and it does not exceed P by more than 50% in about 5/6 of these cells.

[24] Areas failing the $Q <= P$ test include parts of the Amazon, the Pacific Northwest of the United States, and the Himalayas. In one sense, this is not surprising; rain gauge densities in the Amazon are low, and rainfall estimates are relatively uncertain in the Pacific Northwest and the Himalayas, where the topography is complex. (Indeed, *Adam et al.* [2006] offer an approach that uses the Budyko equation to account for the underestimation of precipitation over topographically complex regions.) We do not claim here, however, that poor rainfall estimates are necessarily responsible for the inconsistencies, because runoff estimates have their own sources of error (section 2.3). Unequivocally identifying which data set is most ''at fault'' in these regions is beyond the scope of this study. The relevant result is that researchers should be cautious about using the ISLSCP-2 precipitation and runoff data together in these regions. The points identified in the plot are excluded from the analyses in section 4 below.

3.3. Points With Hydrologically Suspicious Behavior

[25] Another 3% of all land grid cells (4% of the cells in the GRDC-corrected area) require special consideration because the water and energy variables at these cells violate a basic assumption of Budyko's analysis: that evaporation not exceed the net radiation. We compute the long-term average evaporation, E, from the ISLSCP-2 data as $E = P - Q$. Figure 3b shows, with dots, the locations where the ISLSCP-2 data fail the $E <= R_{net}/\lambda$ test. This occurs, for example, on the southern coast of Alaska and across parts of northern Europe. Note that if we had scaled the net radiation (see section 2.2) by the latent heat of sublimation rather than by the latent heat of vaporization in latitudes poleward of 40°, to account (rather overconservatively) for the presence of snow, the points failing the $E <= R_{net}/\lambda$ test would increase to 5% of all land grid cells (10% of the cells in the GRDC-corrected area). Again, though, the main results of the analysis below would remain unchanged.

[26] Note that having E exceed R_{net}/λ is not necessarily incorrect, since the energy needed to evaporate water could come from a negative sensible heat flux (effectively, from external warm air advected over an area) as well as from the net radiation. (Indeed, for northern Europe, *Milly and Dunne* [2002] faced the same problem and questioned the correctness of the $E <= R_{net}/\lambda$ assumption there.) Still, the violation of the $E <= R_{net}/\lambda$ condition does seem to point to ISLSCP-2 data inconsistencies in western tropical South America, for which sensible heat flux is presumably positive throughout the year. Given the inconsistency with the Budyko framework, these grid cells are not included in the analyses of section 4.

[27] A larger subset of the land grid cells, roughly 13% of all land points (20% in the GRDC Area), are identified as having another form of suspicious behavior: the standard deviation of yearly runoff, σ_Q, at these points exceeds that of the yearly precipitation, σ_P. These points are located with dots in Figure 3c. We must emphasize that a $\sigma_Q <= \sigma_P$ criterion is somewhat subjective, since it is not based on water balance considerations. Conceivably, for example, a region could receive the same total precipitation every year ($\sigma_P = 0$) but have a nonzero runoff variability ($\sigma_Q > 0$) because of interannual variations in the subyearly temporal distribution of the precipitation. In addition, with σ_Q and σ_P computed from a small number of annual totals, the $\sigma_Q < \sigma_P$ criterion could be violated through sampling error alone. Still, given that annual precipitation is the main driver of annual runoff, so that interannual precipitation variability is a first-order driver of interannual runoff variability, and given that soil can act as a low-pass filter, so that higher frequencies of precipitation are partially filtered out in the translation of precipitation to runoff, the $\sigma_Q < \sigma_P$ criterion is not unreasonable. The points indicated in Figure 3c can therefore be deemed suspicious: The yearly variations in the ISLSCP-2 precipitation and runoff data sets are likely to be inconsistent in these regions, and thus the annual means derived from these yearly values are also questionable. Some of the analyses in section 4 are performed with and without the $\sigma_Q <= \sigma_P$ criterion applied.

3.4. Time Period Considered

[28] The ISLSCP-2 data set nominally covers the period 1986–1995. The final year of the data set, however, included some missing data. For this reason, all calculations were limited to the time period 1986–1994.

4. Relevance of Budyko's Relationships for Modern, Global Data

4.1. Global Fields of Dryness Index

[29] Figure 4a shows the global distribution of Budyko's dryness index, *D*, as computed from ISLSCP-2 precipitation

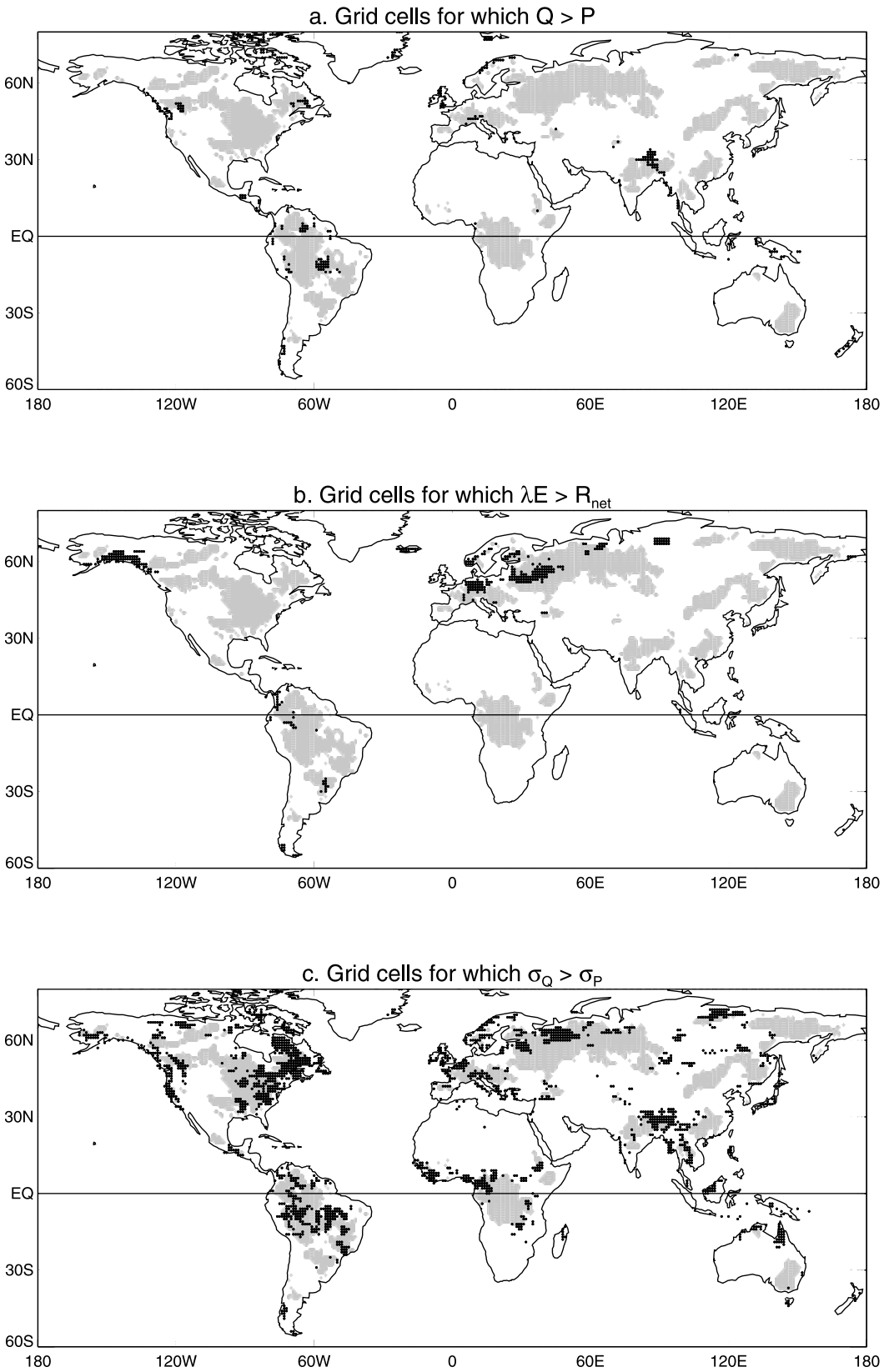

Figure 3. (a) Locations (dots) for which ISLSCP-2 annual runoff values exceed ISLSCP-2 annual precipitation values, implying hydrological inconsistency in the data. (b) Locations for which the annual evaporation rate (as derived from ISLSCP-2 annual precipitation and runoff rates) exceeds the amount allowed by the net radiation, R_{net}/λ. (c) Locations for which the standard deviation of annual runoff in the ISLSCP-2 data set exceeds that of annual precipitation in that data set. In all panels, the location of the "GRDC area" from Figure 2 is shaded.

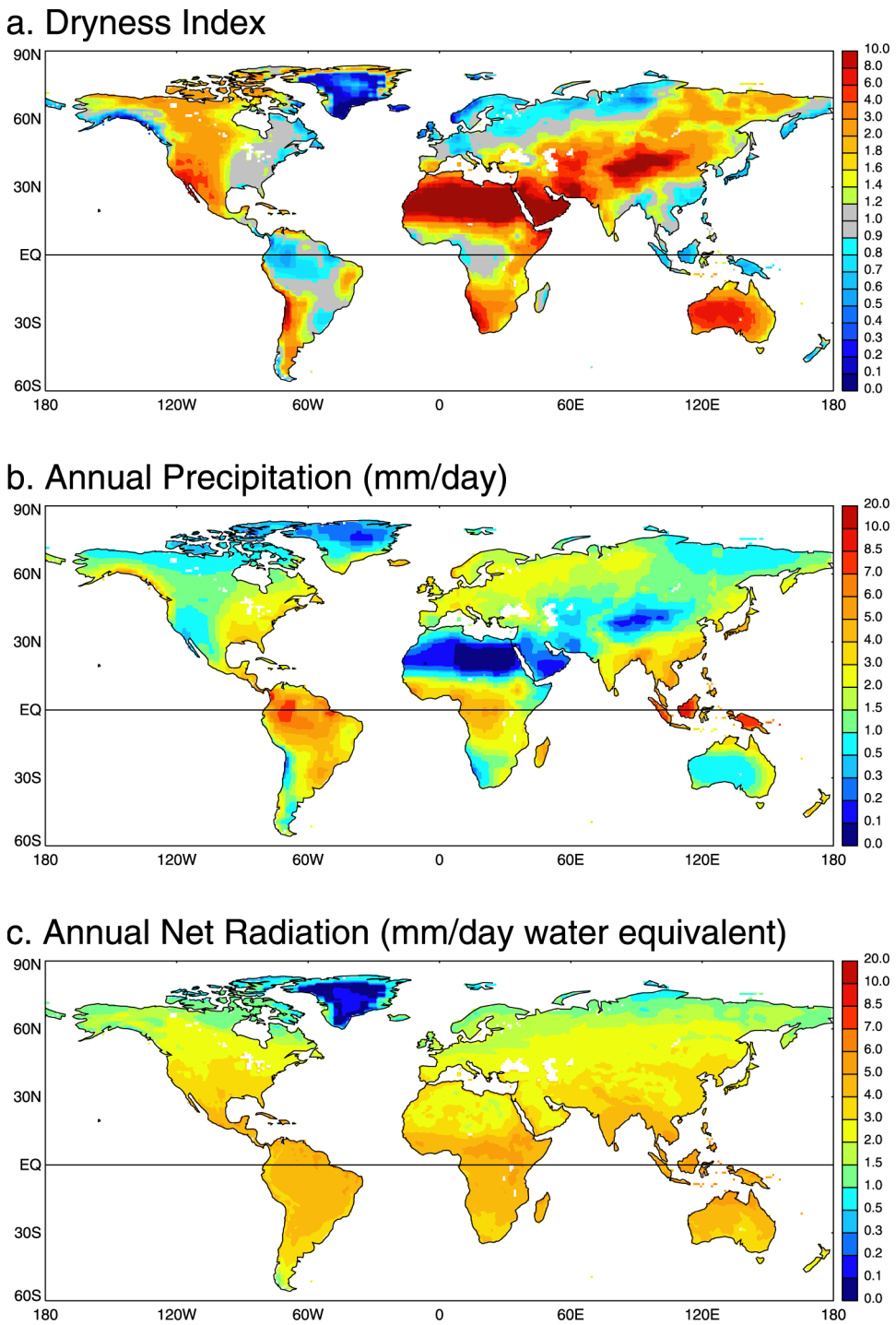

Figure 4. (a) Dryness index, as computed from the long-term annual means of precipitation and net radiation in the ISLSCP-2 data set. (b) Long-term annual mean of precipitation, from ISLSCP-2. (c) Long-term annual mean of net radiation (in terms of water equivalent), from ISLSCP-2.

and net radiation fields. D exceeds 1 over a majority of the Earth's land surface, implying (according to Budyko's treatment) that water availability rather than energy availability controls most land surface evaporation. Locations, however, for which energy availability is most important include the Amazon, Southeast Asia and Indonesia, and the northern edge of Europe and central Asia. Intermediate regions, for which energy and water availability play similar roles, include the eastern half of North America, subtropical South America, tropical Africa, and much of Europe.

[30] Figure 4a provides a unique, observations-based global map of a first-order hydroclimatological control over evaporation (and, by extension, runoff), a map that should prove valuable for understanding the global water cycle and for evaluating its simulation by climate models. The annual water balance is, after all, effectively controlled by precip-

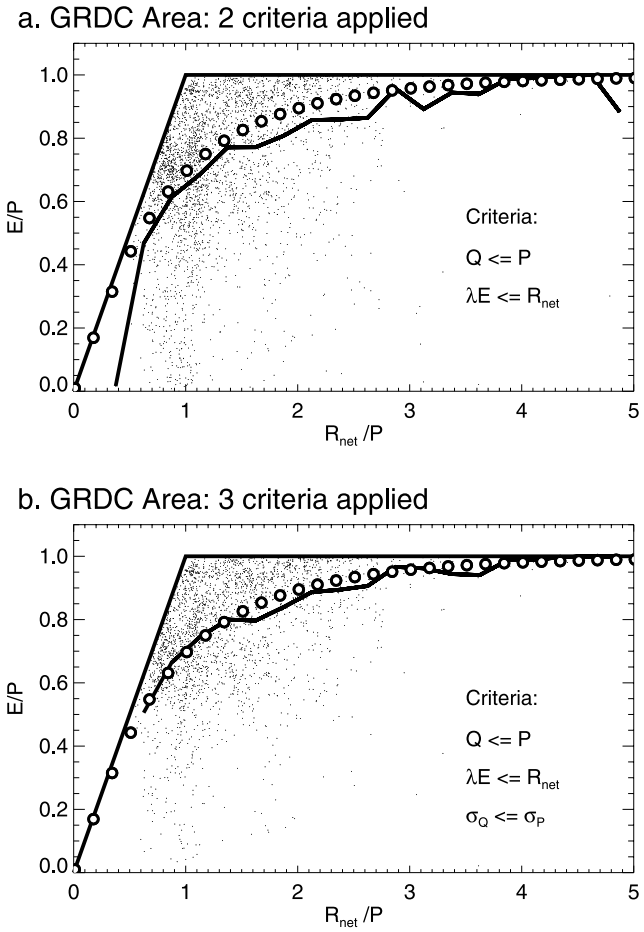

Figure 5. (a) Scatterplot showing, for the ISLSCP-2 data, how the ratio of annual evaporation to precipitation varies with dryness index. Each point in the plot represents a $1° \times 1°$ grid cell lying within the GRDC-corrected area in Figure 2 and satisfying the $Q < P$ and $E < R_{net}/\lambda$ criteria. The solid bin curve shows the average relationship between the data, and the open circles show the original Budyko relationship, from Figure 1. (b) Same as Figure 5a but removing from the analysis the grid cells for which $\sigma_Q > \sigma_P$.

itation and net radiation acting jointly, so that a look at either field alone would prove less instructive. *Koster et al.* [2000a, Figure 11] show a map of climate model-simulated dryness index that differs from Figure 4a in several areas, including over northeastern Asia, where the simulated values appear much too low. These simulated values are for a longer time period (several decades rather than the nine years considered here), so the differences may be due in part to decadal-scale climate fluctuations that would have a larger impact on the signal in the ISLSCP data. We note, however, that a supplemental analysis of GPCP data for the period 1979–2000 suggests that the ISLSCP period is not strongly anomalous: Outside of desert regions, the differences between rainfall in the ISLSCP period and that of the full 22-year period are generally below 5%. The differences are more likely explained by biases in the model. The model's simulation of evaporation, and even the ratio of evaporation to precipitation, in regions such as northeastern Asia would likely be poor even if the land model employed were perfect. The hydroclimatology of any global model can be similarly evaluated.

[31] Figures 4b and 4c show the corresponding ISLSCP-2 mean annual precipitation and net radiation fields (the latter scaled by the latent heat of vaporization, λ, to produce water-equivalent units). As might be expected, the D field's patterns largely match those of the precipitation field, since net radiation has fewer spatial variations. The net radiation, however, does have a strong latitudinal gradient, a gradient that is folded into D.

4.2. Reproduction of Budyko's Curve

[32] The two scatterplots in Figure 5 show the relationship between E/P and D under two different sets of criteria. In Figure 5a, the relationship is shown for GRDC-corrected data that satisfy the $Q <= P$ and $\lambda E <= R_{net}$ criteria discussed in section 3. As before, E is estimated as $P - Q$. Overlain on the scatterplot is a bin curve (the solid curve) showing the average relationship between the variables; the E/P values for all D values within a given range (bin width = 0.25) were averaged to compute the corresponding point in the bin curve. The open circles show the expected relationship from Budyko, computed with (1). Note that when Budyko developed his curve using observations, he also used a binning procedure to filter out scatter.

[33] The bin curve and the Budyko curve have the same basic shape, suggesting that Budyko's reasoning regarding rainfall and net radiation controls on annual evaporation, and their different levels of importance in different hydroclimatological regimes, is fully supported by the data. Note, though, that the bin curve falls slightly below the Budyko curve. This implies that either Budyko's simple semiempirical framework is slightly deficient or that the ISLSCP-2 precipitation, net radiation, and runoff data sets are slightly inconsistent. Curiously, *Milly and Dunne* [2002] found the opposite result for their larger-scale basins; in their analysis, the Budyko curve underestimated the inferred observational evaporation. They suggested the possibility that precipitation underestimates (due, for example, to gauge undercatch) may have hampered Budyko's ability to produce an accurate fit. The ISLSCP precipitation estimates, however, account for undercatch and should not show significant negative biases.

[34] Figure 5b shows the same analysis, but with some additional points excluded: the 20% of the points for which $\sigma_Q > \sigma_P$ (see Figure 3c). As discussed in section 2, because year-to-year variability in precipitation is the chief driver of year-to-year variability in runoff, the condition $\sigma_Q > \sigma_P$, while not rigorously incorrect, nevertheless suggests that the underlying data sets may be inconsistent. When the $\sigma_Q < \sigma_P$ criterion is applied, i.e., when these suspicious points are excluded, the agreement between the Budyko and ISLSCP curves becomes stronger.

[35] Naturally, any conclusion regarding the agreement between the curves requires some qualification. Budyko did not have access to the wealth of data provided by ISLSCP-2, and thus sampling error alone on his part may be responsible for the differences in Figure 5a. The removal of additional ISLSCP-2 points in Figure 5b, many of which appear to be outliers, may be compensating for his sampling error. In other words, it is possible that the Earth's true

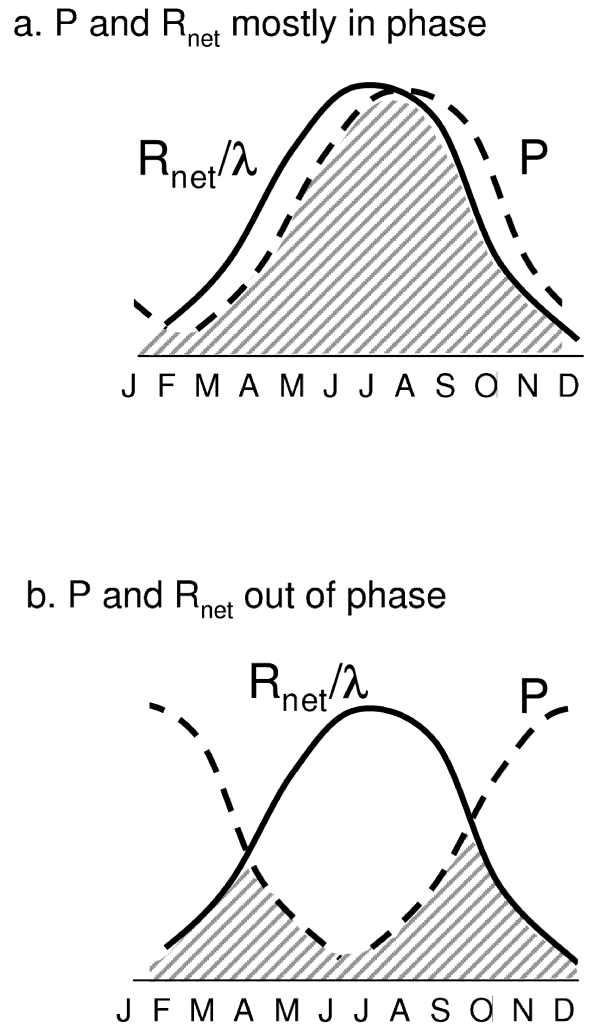

Figure 6. Idealized schematic of two contrasting regions: (a) one for which the precipitation and net radiation cycles are mostly in phase and (b) the other for which they are mostly out of phase. The crosshatched area represents the integral over time of the minimum (at any given month) of the two cycles.

underlying relationship between E/P and dryness index does not match the Budyko curve. (Perhaps it looks more like the ISLSCP-2 curve in Figure 5a.) Still, the agreement in Figure 5b is strong, and the criterion for excluding the additional points in Figure 5b is reasonable. Thus, with the above caveat, Figure 5b suggests that, according to present-day, state-of-the-art global observations, Budyko's semiempirical fit to water balance behavior in selected basins does hold true on the global scale.

4.3. Phase Differences in the Seasonal Cycles of the Forcing

[36] The Budyko relationship provides the "average" value of E/P for a wide range of basin-scale regions with a given dryness index. It is not meant to give an accurate value of the ratio at a single point or region. Figure 5 shows a tremendous amount of scatter about the Budyko function. Reasons for the scatter, for why two locations with the same dryness index partition rainfall in different ways, are many. For example, even with the same D, regions may differ in their vegetation structure, which affects the effective resistance applied to evaporation; in their topography or soil character, which affect their ability to generate runoff; and in the high-frequency structure of the precipitation, which also affects runoff.

[37] The ISLSCP-2 precipitation and radiation data afford a look at an additional, potentially important source for the scatter, namely, the relative phasing of the seasonal cycles of the precipitation and net radiation forcing. Consider the two sets of seasonal cycles in Figure 6. In Figure 6a, the P and R_{net} cycles are largely in phase, whereas in Figure 6b, the two cycles are out of phase. According to an overly strict interpretation of the Budyko relationship, the evaporation rate for the two cases would be the same, since the annual precipitation and net radiation, and thus the dryness index, for the two cases are exactly the same. Recall, however, that evaporation requires the presence of both water (through P) and energy (through R_{net}). The crosshatched area in each panel lies below the minimum of P and R_{net} at each month and thus represents the evaporation rate possible assuming no interseasonal storage of moisture or energy. The evaporation is larger (and thus runoff is smaller) when the two seasonal cycles are more in phase, despite the equivalent dryness index.

[38] Of course, this argument is flawed because the interseasonal storage of moisture (through snowpack and soil moisture reservoirs) is known to be very important [e.g., *Milly and Dunne*, 1994]. Still, the relative phasing of the cycles may have some impact on runoff, and we can search for this impact in the ISLSCP data. Table 1 shows the degree to which phasing affects the observed runoff within narrow ranges of the dryness index. The phasing diagnostic used here, computed separately at each grid cell, is the area of the crosshatched region in Figure 6 divided by whichever is smaller: the total annual precipitation or the total annual net radiation. It thus varies from 0 to 1, with lower values implying that the precipitation and net radiation cycles are more out of phase. The runoff diagnostic is simply the ratio of observed annual runoff to observed annual precipitation. The second column of the table shows the correlation (r) between the phasing diagnostic and the runoff diagnostic. The third column shows the number of points (N) that went into the calculation (i.e., lying within the dryness index range) and the probability, in percent, that the underlying true correlation is not zero (based on Monte Carlo analysis, in which 30,000 pairs of independent, randomly generated data sets of length N are compared to each other). The final column shows the mean of the phasing diagnostic, which hovers around 0.8 for the different bins. (Note that the higher mean values for the lower bins are consistent with the construct of the diagnostic; when either $P \gg R_{net}/\lambda$ or $R_{net}/\lambda \gg P$, the phasing diagnostic tends to go to 1.) The analysis is limited to points falling within GRDC basins and to points between 40°N and 40°S, to avoid known storage issues associated with snow in higher latitudes. Only ranges containing at least 50 points are included in the table. To maximize the number of points considered, the analysis

Table 1. Correlations Between Phase Index and Runoff Index for Various Dryness Index Intervals[a]

Dryness Index Range	Correlation Between Phase Index and Runoff Index	Number of Points (and Statistical Significance)	Average of Phase Index
$0.7 < D < 0.8$	−0.077	127 (80%)	0.87
$0.8 < D < 0.9$	−0.706	136 (99.99+%)	0.84
$0.9 < D < 1.0$	−0.285	161 (99.98%)	0.80
$1.0 < D < 1.1$	−0.563	220 (99.99+%)	0.80
$1.1 < D < 1.2$	−0.474	144 (99.99+%)	0.81
$1.2 < D < 1.3$	−0.261	82 (99.14%)	0.81
$1.3 < D < 1.4$	−0.241	66 (97.4%)	0.82

[a]See text for details.

applied the $Q < P$ and $E < R_{net}$ criteria but did not apply the $\sigma_Q < \sigma_P$ criterion.

[39] As expected, the correlations between the phasing diagnostic and the runoff ratio are negative, with a large degree of statistical significance. In other words, despite their disparate sources, the observational data do provide evidence that annual runoff is affected by the relative phasing of the cycles of water supply and energy supply at the land surface. Note, however, that the correlations in Table 1, though significant, are not large. There are two likely reasons for this. First, the underlying correlations in nature may be small; the other factors contributing to the scatter, as noted above, may be dominant, and in any case the interseasonal storage of water, even in snow-free regions, may ameliorate the effect of the phase differences. Second, of course, the ISLSCP-2 data sets may be inconsistent in places.

[40] For perspective, we can address the phasing question with a global modeling study, one that uses parameterized land surface physics to generate runoff and evaporation fields in response to observed precipitation and net radiation forcing. Such models, of course, are notorious for their biases and their suboptimal parameterizations, but they do provide consistent estimates of P, R_{net}, E, and Q. As part of GSWP-2 (the Global Soil Wetness Project, Phase 2 [see *Dirmeyer et al.*, 2005]), the catchment model [*Koster et al.*, 2000b] of the NASA Goddard Space Flight Center's Global Modeling and Assimilation Office was driven globally offline with realistic meteorological forcing. The correlations between the phasing diagnostic and the simulated runoff ratio were found to be similar to those in Table 1. The GSWP-2 model result suggests that the ISLSCP-2 observations are consistent enough to capture most of the impact of phasing on the water budget, small as it might be.

4.4. Interannual Variability

[41] To examine the consistency between the year-to-year variations in the ISLSCP-2 precipitation and runoff data, we could compute correlations between monthly or annual values. This approach, however, cannot account for the fact that runoff tends to lag precipitation. Precipitation falling at the end of one calendar year may run off at the beginning of the next, sometimes throwing off the correlation significantly. Attempts to correct for this would require a subjective grid cell by grid cell analysis, which is beyond the scope of this paper.

[42] The approach of *Koster and Suarez* [1999], however, is suitable for the present study, since it can be reformulated to rely strictly on the standard deviations of rainfall and runoff (σ_P and σ_Q, respectively) without consideration of their correlation. A reformulation of (2), the equation used by *Koster and Suarez* [1999], is necessary because estimates of σ_E require yearly estimates of evaporation, estimates that are prevented by the lagged behavior of the runoff. Equation (2) is thus rewritten as:

$$\sigma_Q/\sigma_P = 1 - \mathcal{F}(D) + DF'(D) \quad (3)$$

[43] Underlying (3) is the idea that a given year's total precipitation and net radiation are enough to determine the partitioning of that year's precipitation into runoff and evaporation. As a result, the framework is inconsistent with the idea that σ_Q can exceed σ_P; indeed, all three criteria used in Figure 5b ($Q <= P$, $\lambda E <= R_{net}$, $\sigma_Q <= \sigma_P$) must be applied to the data before evaluating their consistency with (3). Figure 7 shows the scatterplot of σ_Q/σ_P versus D for the ISLSCP-2 data in the GRDC area, applying the three criteria. The bin curve representing the average relationship is also shown, as is the curve representing (3).

[44] Once again, the agreement, while not perfect, is strong. Our ability to examine the consistency of year-to-

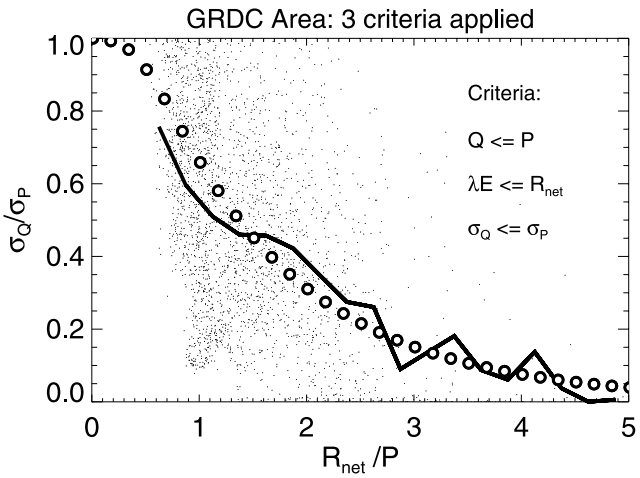

Figure 7. Scatterplot showing, for the ISLSCP-2 data, how the ratio of the standard deviation of annual runoff to that of annual precipitation varies with dryness index. Each point in the plot represents a $1° \times 1°$ grid cell lying within the GRDC-corrected area in Figure 2 and satisfying the $Q < P$, $E < R_{net}/\lambda$, and $\sigma_Q < \sigma_P$ criteria. The solid bin curve shows the average relationship between the data, and the open circles show the original Budyko-based relationship, from Figure 1.

year variations in the ISLSCP-2 data sets is very limited, but to the extent that we can test it, and outside of the indicated areas for which $\sigma_Q > \sigma_P$, the data sets appear generally consistent in the context of the Budyko framework.

5. Summary

[45] The ISLSCP-2 data set provides coregistered global fields of three fundamental elements of the global hydrological cycle: precipitation (P), net radiation (R_{net}), and runoff (Q). From the mean annual P and R_{net} fields, we can compute an observations-based global distribution (Figure 4a) of Budyko's dryness index (D), known to be a first-order control on global evaporation and runoff fields. This D field by itself should prove invaluable to global modelers wishing to evaluate strengths and deficiencies in their simulation of the global hydrological cycle.

[46] The P, R_{net}, and Q fields in the ISLSCP data set, however, come from independent measurement systems, particularly the portion of the Q fields lying within GRDC-corrected basins (Figure 2). Thus we might expect to see some inconsistency between the fields. In some grid cells, runoff exceeds precipitation, a clear violation of the long-term water balance (Figure 3a). Inferred evaporation rates exceed net radiation rates in a number of grid cells (Figure 3b), and while this does not strictly violate the long-term energy budget, since external, advected energy can be transferred to the land surface through a downward sensible heat flux, the data sets' consistency in the tropical and subtropical subset of these regions is strongly suspect. Consistency is also suspect at those locations for which the standard deviation of runoff exceeds that of precipitation (Figure 3c), since annual rainfall variability is the chief driver of annual runoff variability.

[47] Focusing on the GRDC-corrected regions in Figure 2, and with all suspicious points removed from the analysis, the observations reproduce quite well Budyko's semiempirical relationship between dryness index and the ratio of annual evaporation to annual precipitation (Figure 5b). Thus, in terms of the Budyko relationship, the precipitation, net radiation, and runoff data in the ISLSCP-2 data set, though obtained from different sources, are generally consistent.

[48] The ISLSCP-2 data also allow a rare global look at a potentially important control on annual runoff, namely, the relative phasing of the mean seasonal cycles of precipitation and net radiation. The data indeed show (Table 1) that when the cycles are more out of phase, annual runoff tends to increase. The interannual variations of the ISLSCP-2 precipitation and runoff data were examined using the Budyko-based framework of *Koster and Suarez* [1999]. The results (Figure 7) show that the disparate data sets are also generally consistent in this context.

[49] Of course, the Budyko curves in Figure 1 are semiempirical and thus do not stem strictly from theory. Also, the scatter around the curves is substantial, diminishing the relevance of the relationships at any individual point or region. Thus it is incorrect to conclude that the agreement with the Budyko curves in Figures 5b and 7 quantitatively validates the ISLSCP-2 fields. Rather, the agreement shows that together, the ISLSCP-2 fields successfully capture the basic (and reasonable) hydroclimatological constraints on evaporation outlined by Budyko: the fact that evaporation is controlled by precipitation in drier climates, by net radiation in wetter climates, and by a more complex set of controls (including the relative phasing of P and R_{net}) in intermediate climates. In short, outside of the identified inconsistent and suspicious points, the independently derived ISLSCP-2 fields appear hydroclimatologically consistent. Conversely, the agreement shows that the decades-old Budyko framework holds up very well when tested with the most up-to-date, spatially complete and highly resolved global observations available. To the extent that the ISLSCP-2 data are valid, the Budyko framework is seen to remain a useful approach for characterizing first-order controls on the global hydrological cycle.

[50] **Acknowledgments.** The authors thank Ping Liu for help with the processing of the ISLSCP data. Forrest Hall and Eric Brown de Colstoun are thanked for their leadership in producing the ISLSCP-2 data set.

References

Adam, J. C., E. A. Clark, D. P. Lettenmaier, and E. F. Wood (2006), Correction of global precipitation products for orographic effects, *J. Clim.*, *19*, 15–38.

Adler, R. F., G. J. Huffman, and P. R. Keehn (1994), Global tropical rain estimates from microwave-adjusted geosynchronous IR data, *Remote Sens. Rev.*, *11*, 125–152.

Adler, R. F., et al. (2003), The version 2 Global Precipitation Climatology Project (GPCP) monthly precipitation analysis (1979-present), *J. Hydrometeorol.*, *4*, 1147–1167.

Budyko, M. I. (1958), *The Heat Balance of the Earth's Surface*, translated by N. A. Stepanova, 259 pp., U.S. Dep. of Commer., Washington, D. C.

Budyko, M. I. (1974), *Climate and Life*, 508 pp., Elsevier, New York.

Charlock, T. P., and T. L. Alberta (1996), The CERES/ARM/GEWEX Experiment (CAGEX) for the retrieval of radiative fluxes with satellite data, *Bull. Am. Meteorol. Soc.*, *77*, 2673–2683.

Cox, S. J., P. W. Stackhouse Jr., S. K. Gupta, J. C. Mikovitz, M. Chiacchio, and T. Zhang (2004), The NASA/GEWEX Surface Radiation Budget Project, results and analysis, paper presented at International Radiation Symposium, Int. Radiat. Comm., Busan, South Korea, 23–27 Aug.

Dirmeyer, P. A., X. Gao, M. Zhao, Z. Guo, T. Oki, and N. Hanasaki (2005), The second Global Soil Wetness Project (GSWP-2): Multi-model analysis and implications for our perception of the land surface, *COLA Tech. Rep. 185*, 46 pp., Cent. for Ocean-Land-Atmos. Stud., Calverton, Md. (Available at ftp://grads.iges.org/pub/ctr/ctr_185.pdf)

Fekete, B. M., C. J. Vörösmarty, and W. Grabs (2002), High resolution fields of global runoff combining observed river discharge and simulated water balances, *Global Biogeochem. Cycles*, *16*(3), 1042, doi:10.1029/1999GB001254.

Gilgen, H., and A. Ohmura (1999), The global energy balance archive, *Bull. Am. Meteorol. Soc.*, *80*(5), 831–850.

Gupta, S. K., N. A. Ritchey, A. C. Wilber, C. H. Whitlock, G. G. Gibson, and P. W. Stackhouse Jr. (1999), A climatology of surface radiation budget derived from satellite data, *J. Clim.*, *12*, 2691–2710.

Hagemann, S., and L. Dümenil (1998), A parameterization of the lateral waterflow for the global scale, *Clim. Dyn.*, *14*, 17–31.

Hall, F. G., E. B. de Colstoun, G. J. Collatz, D. Landis, P. Dirmeyer, A. Betts, G. J. Huffman, L. Bounoua, M. Bosilovich, and B. Meeson (2006), The ISLSCP Initiative II global data sets: Surface boundary conditions and atmospheric forcings for land-atmosphere studies, *J. Geophys. Res.*, doi:10.1029/2006JD007366, in press.

Koster, R. D., and M. J. Suarez (1999), A simple framework for examining the interannual variability of land surface moisture fluxes, *J. Clim.*, *12*, 1911–1917.

Koster, R. D., M. J. Suarez, and M. Heiser (2000a), Variance and predictability of precipitation at seasonal-to-interannual timescales, *J. Hydrometeorol.*, *1*, 26–46.

Koster, R. D., M. J. Suarez, A. Ducharne, M. Stieglitz, and P. Kumar (2000b), A catchment-based approach to modeling land surface processes in a general circulation model: 1. Model structure, *J. Geophys. Res.*, *105*, 24,809–24,822.

Koster, R. D., P. A. Dirmeyer, P. C. D. Milly, and G. L. Russell (2001), Comparing GCM-generated land surface water budgets using a simple common framework, in *Land Surface Hydrology, Meteorology, and Climate: Observations and Modeling*, *Water Sci. and Appl. Ser.*, vol. 3, edited by V. Lakshmi, pp. 95–105, AGU, Washington, D. C.

Milly, P. C. D., and K. A. Dunne (1994), Sensitivity of the global water cycle to the water-holding capacity of land, *J. Clim.*, *7*, 506–526.

Milly, P. C. D., and K. A. Dunne (2002), Macroscale water fluxes: 2. Water and energy supply control of their interannual variability, *Water Resour. Res.*, *38*(10), 1206, doi:10.1029/2001WR000760.

New, M., M. Hulme, and P. Jones (1999), Representing twentieth century space-time climate variability. Part I: Development of a 1961–1990 mean monthly terrestrial climatology, *J. Clim.*, *12*, 829–856.

New, M., M. Hulme, and P. Jones (2000), Representing twentieth century space-time climate variability. Part II: Development of 1901–1996 monthly grids of terrestrial surface climate, *J. Clim.*, *13*, 2217–2238.

Ohmura, A., et al. (1998), Baseline Surface Radiation Network (BSRN/WCRP): New precision radiometry for climate research, *Bull. Am. Meteorol. Soc.*, *79*(10), 2115–2136.

Pinker, R., and J. A. Ewing (1985), Modeling of surface solar radiation: Model formulation and validation, *J. Clim. Appl. Meteorol.*, *24*, 389–401.

Rantz, S. E., et al. (1982), Measurement and computation of streamflow, vol. 2, Computation of discharge, *U. S. Geol. Surv. Water Supply Pap. 2175*, 347 pp.

Rossow, W. B., and R. Schiffer (1999), Advances in understanding clouds from ISCCP, *Bull. Am. Meteorol. Soc.*, *80*, 2261–2287.

Rossow, W. B., A. W. Walker, D. E. Beuschel, and M. D. Roiter (1996), International Satellite Cloud Climatology Project (ISCCP) documentation of new cloud datasets, *WMO/TD 737*, 115 pp., World Clim. Res. Programme, Geneva, Switzerland.

Schubert, S., C.-K. Park, C.-Y. Wu, W. Higgins, Y. Kondratyeva, A. Molod, L. Takacs, M. Seablom, and R. Rood (1995), A multi-year assimilation with the GEOS-1 system: Overview and results, *NASA Tech. Memo. 104606*, vol. 6.

Stackhouse, P. W., Jr., S. K. Gupta, S. J. Cox, J. C. Mikovitz, T. Zhang, and M. Chiacchio (2004), 12-year surface radiation budget data set, *GEWEX News*, *14*(4), 10–12.

Wilber, A. C., D. P. Kratz, and S. K. Gupta (1999), Surface emissivity maps for use of satellite retrievals of longwave radiation, *NASA Tech. Publ., TP-99-209362*, 35 pp.

Zhang, Y.-C., W. B. Rossow, A. A. Lacis, V. Oinas, and M. I. Mishchenko (2004), Calculation of radiative fluxes from the surface to top-of-atmosphere based on ISCCP and other global data sets: Refinements of the radiative transfer model and the input data, *J. Geophys. Res.*, *109*, D19105, doi:10.1029/2003JD004457.

Zhang, Y., W. B. Rossow, and P. W. Stackhouse Jr. (2006), Comparison of different global information sources used in surface radiative flux calculation: Radiative properties of the near-surface atmosphere, *J. Geophys. Res.*, *111*, D13106, doi:10.1029/2005JD006873.

B. M. Fekete, Water Systems Analysis Group, Complex Systems Research Center, Institute for the Study of Earth, Oceans, and Space, University of New Hampshire, Morse Hall, Durham, NH 03824, USA.

G. J. Huffman, Science Systems and Applications, Inc., Code 613, NASA Goddard Space Flight Center, Greenbelt, MD 20771, USA.

R. D. Koster, Global Modeling and Assimilation Office, Code 610.1, NASA Goddard Space Flight Center, Greenbelt, MD 20771, USA. (randal.d.koster@nasa.gov)

P. W. Stackhouse Jr., NASA Langley Research Center, 21 Langley Boulevard, M.S. 420, Hampton, VA 23681, USA.